

# Consistent eccentricities for gravitational wave astronomy: Resolving discrepancies between astrophysical simulations and waveform models

Aditya Vijaykumar,<sup>1,2,\*</sup> Alexandra G. Hanselman,<sup>3</sup> and Michael Zevin<sup>4,5,6,7</sup>

<sup>1</sup>*Canadian Institute for Theoretical Astrophysics, University of Toronto, 60 St George St, Toronto, ON M5S 3H8, Canada*

<sup>2</sup>*International Centre for Theoretical Sciences, Tata Institute of Fundamental Research, Bangalore 560089, India*

<sup>3</sup>*Department of Physics, The University of Chicago, 5640 South Ellis Avenue, Chicago, Illinois 60637, USA*

<sup>4</sup>*Kavli Institute for Cosmological Physics, The University of Chicago, 5640 South Ellis Avenue, Chicago, Illinois 60637, USA*

<sup>5</sup>*Enrico Fermi Institute, The University of Chicago, 933 East 56th Street, Chicago, Illinois 60637, USA*

<sup>6</sup>*Adler Planetarium, 1300 South DuSable Lake Shore Drive, Chicago, IL, 60605, USA*

<sup>7</sup>*Center for Interdisciplinary Exploration and Research in Astrophysics (CIERA), Northwestern University, Evanston, IL, 60201, USA*

Detecting imprints of orbital eccentricity in gravitational wave (GW) signals promises to shed light on the formation mechanisms of binary black holes. To constrain formation mechanisms, distributions of eccentricity derived from numerical simulations of astrophysical formation channels are compared to the estimates of eccentricity inferred from GW signals. We report that the definition of eccentricity typically used in astrophysical simulations is inconsistent with the one used while modeling GW signals, with the differences mainly arising due to the choice of reference frequency used in both cases. We also posit a prescription for calculating eccentricity from astrophysical simulations by evolving ordinary differential equations obtained from post-Newtonian theory, and using the dominant ( $\ell = m = 2$ ) mode's frequency as the reference frequency; this ensures consistency in the definitions. On comparing the existing eccentricities of binaries present in the Cluster Monte Carlo catalog of globular cluster simulations with the eccentricities calculated using the prescription presented here, we find a significant discrepancy at  $e \gtrsim 0.2$ ; this discrepancy becomes worse with increasing eccentricity. We note the implications this discrepancy has for existing studies, and recommend that care be taken when comparing data-driven constraints on eccentricity to expectations from astrophysical formation channels.

## I. INTRODUCTION

Definitive measurement of orbital eccentricity in a compact binary coalescence (CBC) signal is one of the most exciting prospects of gravitational wave (GW) astrophysics. Despite  $\mathcal{O}(100)$  binary black hole (BBH) signals being detected by the LIGO–Virgo–KAGRA (LVK) network [1–5] to date [6], the distinct pathways that led to the formation and merger of these BBH signals remains a mystery. Measurements of masses, spins, and redshift evolution have helped to identify broad constraints on the underlying physical processes that lead to BBH formation [7], although measurement uncertainties paired with the inherent uncertainties embedded within formation channel modeling make it difficult to use these measurables to robustly pin down the formation pathway for a single BBH or the relative fraction of BBHs that results from one formation channel compared to another (see e.g. [8, 9]).

Measurable orbital eccentricity in stellar-mass BBH mergers, on the other hand, has been shown to be a robust indicator that a particular BBH signal resulted from a small subset of viable channels [10–35]. Eccentricity is efficiently damped as a compact binary system inspirals and loses energy and angular momentum through GW emission [36]. To retain any measurable semblance of orbital

eccentricities at frequencies accessible to current ground-based GW detectors, a BBH system therefore must be able to form at a high eccentricity ( $\gtrsim 0.9$ ) and merge on an extremely rapid timescale ( $\lesssim 1$  yr, see Ref. [25]) or have some mechanism that continually pumps eccentricity into an inspiraling system (e.g., the von Zeipel-Lidov-Kozai mechanism, [37–39]).

The former of these possibilities is something that can only be attained through strong dynamical encounters within dense stellar environments, such as globular clusters, nuclear clusters, and the disks of active galactic nuclei. The synthesis of eccentric BBHs mergers in globular clusters is a robust and unavoidable result of simple physical processes such as two-body relaxation and (chaotic) gravitational encounters between three or more black holes within the cluster core (see e.g. [16]). Since the relative fraction of systems that proceed through this eccentric subchannel is relatively robust to uncertainties in cluster environments, the detection and measurement of even a small number of eccentric BBH mergers can lead to stringent constraints on the relative fraction of merging BBH systems that result from dynamical environments entirely [30].

Although eccentricity is a powerful constraint on formation pathways in theory, in practice the measurement and interpretation of an eccentric GW signal is much more muddled. Current matched-filter CBC searches applied to GW data [7] only use aligned-spin and quasi-circular templates [40–42], and thus a selection effect exists against detecting eccentric GW signals. The selection function

\* aditya@utoronto.ca

for eccentric systems due to this method for searching the data has yet to be adequately characterized (see discussion in Ref. [30]). Waveform-independent searches for eccentric mergers have also been carried out [43, 44] with no significant triggers; this is unsurprising, since these searches are typically only sensitive to short duration (i.e. high mass) systems. A number of eccentric waveform approximants have been built (e.g. [45–49]), although much more work needs to be done to make them accurate over a large range of eccentricities. In particular, simultaneously modeling eccentricity and spin precession has proved to be challenging (see Ref. [50] for a recent attempt<sup>1</sup>), and these properties have degenerate effects on the GW waveform making it difficult to distinguish between precessing and eccentric hypotheses especially for massive signals [52–54]. Lastly, the definition of eccentricity differs between GW waveform models. Eccentricity evolves during the inspiral of a binary, and hence can only be defined with reference to an epoch in the orbit of that binary. However, the definition of this reference epoch and of eccentricity itself is inconsistent across different state-of-the-art eccentric waveform approximants. There have been attempts towards bringing all these definitions on an equal footing [48, 55–57], allowing consistent comparison of eccentricities derived from diverse waveform approximants.

A robust and consistent definition for eccentricity that is shared across waveform models and astrophysical models is imperative to yield any astrophysical conclusions in the event of an eccentric BBH detection. In this paper, we show that the definition of eccentricity currently employed in astrophysical models is different from the definition used in waveform models. We also paint a clearer picture as to where these discrepancies in the definition of eccentricity lie, and present a framework for determining a robust definition of eccentricity that can be utilized for self-consistent comparisons between predictions from the astrophysical modeling community and the GW waveform community.

Our paper is structured as follows. In Section II, we review current methods that are used for defining eccentricity, both in astrophysical simulations and waveform modeling. Section III presents a standardized definition of eccentricity and a scheme for extracting this definition of eccentricity from astrophysical simulations for a direct comparison to GW waveforms. We also show how quoted eccentricity values significantly differ when a self-consistent definition of eccentricity is not used, investigate the robustness of our improved definition to higher-order post-Newtonian (PN) effects and spin, and discuss how our self-consistent picture of eccentricity affects the inferred fraction of measurably eccentric sources from astrophysical models. Finally, we provide a summary and concluding remarks in Section IV. Example python scripts are

available at <https://github.com/adivijaykumar/standard-eccentricity-scripts>, and data products are available on Zenodo [58].

### A. Definitions of eccentricity used in this work

This work refers to eccentricity in many different contexts. For ease of reading, we provide a list of these below.

1.  $e_{W03}$ : Eccentricities calculated from the prescription outlined in [59]. This prescription has been commonly used to extract eccentricities from astrophysical simulations of binary formation (e.g. [14, 16, 18, 25, 30, 60, 61]). As we shall see in Section II B, this prescription uses the GW peak frequency as the reference frequency.
2.  $e_t^{kPN}$ : The eccentricity computed by evolving PN equations accurate to the  $k$ -th order (see e.g. [45, 62]). This uses 22 mode GW frequency as the reference frequency.
3.  $e_{W03}^{f_{22}}$ : Eccentricities calculated using the W03 prescription, but extracted at fixed 22 mode frequency.
4.  $e_{gw}^{wf}$ : Eccentricity definition proposed in [57], computed from a gravitational waveform using the `gw_eccentricity` package (see also Ref. [48]).
5.  $e_0$ : Eccentricity at a given reference point from astrophysical simulations, which is used as an initial condition (along with initial separation  $a_0$ ) to evolve the system to a reference point suitable for GW detectors.

## II. BACKGROUND

### A. Peak harmonic of a GW signal in presence of eccentricity

At least in the inspiral phase of the binary, i.e. when the dynamics is well-described by PN expansion, a binary emits GWs at harmonics of its orbital frequency  $f_{orb}$ ,

$$f_{GW,n} = n f_{orb} \quad ; \quad n \geq 2 \quad .$$

Note that the harmonic index  $n$  is different from the  $(\ell, m)$  basis used to parametrize GW polarizations. At leading order, power emitted by the  $n$ -th harmonic is given by [64],

$$P_n = \frac{32}{5} \frac{G^4}{c^5} \frac{m_1^2 m_2^2 M}{a^5} g(n, e), \quad (1)$$

where the function  $g(n, e)$  quantifies the enhancement in the power emitted in the  $n^{\text{th}}$  harmonic compared to a

<sup>1</sup> See also Ref. [51] that constructs an approximant that includes eccentricity and precession for binaries detectable with LISA

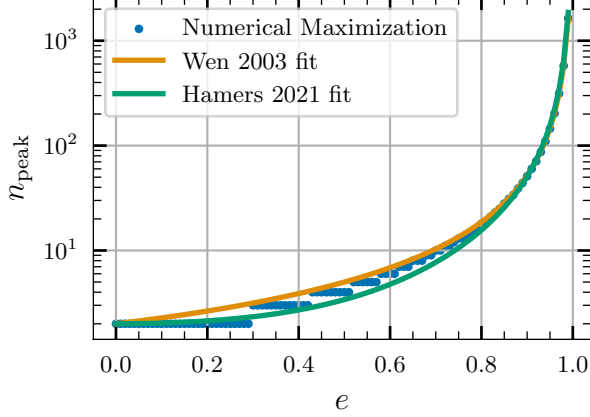


Figure 1. Numerical solution of Eq. (1) for the peak harmonic plotted along with the analytical fits from Ref. [59] and Ref. [63]. We see that the peak harmonic increases with eccentricity, and reaches values  $> 100$  for  $e > 0.9$ . We also see that the fit in Ref. [63] fits the numerical solution better, especially at lower values of eccentricity.

circular orbit (where there is no emission at  $n > 2$ ), and is given by

$$g(n, e) = \frac{n^4}{32} \left\{ \left[ J_{n-2}(ne) - 2eJ_{n-1}(ne) + \frac{2}{n}J_n(ne) + 2eJ_{n+1}(ne) - J_{n+2}(ne) \right]^2 + (1 - e^2) \left[ J_{n-2}(ne) - 2J_n(ne) + J_{n+2}(ne) \right]^2 + \frac{4}{3n^2}J_n(ne)^2 \right\}. \quad (2)$$

Here,  $J_k(x)$  refers to Bessel functions of the first kind. For a given eccentricity, the peak power is emitted at a harmonic where  $g(n, e)$  has the maximum value. For ease of calculation, Ref. [59] provided a fit to the peak harmonic as a function of eccentricity,

$$n_{\text{peak}}^{\text{Wen}}(e) = 2 \frac{(1 + e)^{1.1954}}{(1 - e^2)^{3/2}}. \quad (3)$$

Ref. [63] noted that the above fit does not work well at low eccentricities, and provided an alternative fit to the peak harmonic,

$$n_{\text{peak}}^{\text{Hamers}}(e) = 2 \left( 1 + \sum_{k=1}^4 c_k e^k \right) (1 - e^2)^{-3/2}. \quad (4)$$

Here,  $c_1 = -1.01678$ ,  $c_2 = 5.57372$ ,  $c_3 = -4.9271$ , and  $c_4 = 1.68506$ . Both these estimates are plotted in Figure 1 along with the peak harmonic calculated numerically.

## B. Eccentricity extraction prescription of Ref. [59]

Since the value of eccentricity changes during the course of the inspiral, the value of eccentricity is often quoted at a specific reference frequency (or reference time). Ref. [59] (henceforth referred to as W03) uses the peak harmonic's frequency as a reference for defining eccentricity, and this definition has been employed by many other studies (e.g. [14, 16, 18, 25, 30, 60, 61]). Given semimajor axis  $a$  and total mass  $M$ , the average orbital frequency  $f_{\text{orb}}$  is

$$f_{\text{orb}} = \frac{1}{2\pi} \sqrt{\frac{GM}{a^3}}. \quad (5)$$

This means that the peak GW frequency is,

$$f_{\text{peak, GW}} = \frac{(1 + e)^{1.1954}}{\pi(1 - e^2)^{3/2}} \sqrt{\frac{GM}{a^3}}. \quad (6)$$

In astrophysical simulations, we are generally interested in obtaining eccentricity at a specified reference frequency, given an initial value of semi-major axis  $a_0$  and eccentricity  $e_0$ . These initial values can be thought of as arising either from some fiducial distribution of eccentricities and separations, or from stopping conditions in dynamical simulations. W03 uses the leading (Newtonian) order evolution [36] of the semi-major axis and eccentricity to relate  $(a_0, e_0)$  to  $(a, e)$  at a different time,

$$\frac{a(1 - e^2)}{e^{12/19}} \left( 1 + \frac{121}{304} e^2 \right)^{-870/2299} = \frac{a_0(1 - e_0^2)}{e_0^{12/19}} \left( 1 + \frac{121}{304} e_0^2 \right)^{-870/2299}. \quad (7)$$

For a given value of the reference frequency  $f_{\text{peak, GW}}$ , the eccentricity can be obtained by solving Eq. (6) and Eq. (7) simultaneously.

## C. Possible issues with the W03 prescription

While the W03 procedure has been used in deriving eccentricities at a particular GW frequency in many simulations, it has a couple of drawbacks:

1. The reference frequency is taken to be the peak frequency of the orbit. This is inconsistent with

recommendations in the literature attempting to standardize the definition of eccentricity in waveforms [48, 57]. Specifically, these works motivate using the orbit-averaged 22 (i.e.  $\ell = 2$ ,  $m = 2$ ) mode frequency as a consistent reference point, on account of its smooth and monotonic evolution over the course of the inspiral.

2. Since all equations are based on Ref. [36], they are restricted to Newtonian (i.e. leading) order. This is not a good approximation of the evolution of the orbit, especially for systems close to merger. Specifically, the ordinary differential equations describing the evolution of eccentricities and the 22 mode frequencies have been calculated to several PN orders beyond the Newtonian order, also with the inclusion of spins. Furthermore, this equation breaks down at very high eccentricity.

In the rest of our paper, we shall formulate a procedure that can be applied to any set of scattering experiments to extract eccentricities, and conduct sanity checks of our procedure. In order to accomplish this, we shall solve the problems listed above<sup>2</sup>.

### III. A CONSISTENT PRESCRIPTION FOR CALCULATING ECCENTRICITY

As shown in Figure 1, the peak harmonic of an eccentric inspiral takes higher values for higher eccentricities.

For low values of eccentricity ( $e \lesssim 0.3$ ), the peak harmonic is  $n_{\text{peak}} = 2$ , and hence the 22-mode frequency is the same as frequency of the peak harmonic. However, the difference between the peak harmonic frequency and the 22-mode frequency increases very quickly, with  $f_{\text{peak}} = 10f_{\text{orb}} = 5f_{22}$  at  $e \approx 0.7$ . This discrepancy means that the eccentricities derived from astrophysical simulations of different binary formation channels is defined at a different reference frequency as compared to the definition of reference frequency built into waveforms as per recommendations of Ref. [57]. As is also evident, this discrepancy is worse for higher eccentricities, which are arguably more interesting from an astrophysical standpoint.

To remedy this discrepancy, the definitions of eccentricity from the simulations and waveforms need to be placed on the same footing. Hence, instead of defining eccentricity at the frequency of the peak harmonic, we define eccentricity at the orbit-averaged 22 mode frequency. Let  $M = m_1 + m_2$  be the total mass of the binary and  $\eta = (m_1 m_2)/M^2$  be the symmetric mass ratio, where  $m_1$  and  $m_2$  are the component binary masses. Given an initial value of semimajor axis  $a_0$  and eccentricity  $e_0$  for a particular binary from a simulation, we evolve differential equations in  $e$  and  $v$  given by PN formulae,

$$\frac{de}{dt} = -\frac{e(121e^2 + 304)\eta v^8}{15M\epsilon^5} [1 + \alpha_2 v^2 + \alpha_3 v^3 + \alpha_4 v^4 + \mathcal{O}(v^5)] \quad (8)$$

$$\frac{dv}{dt} = \frac{(37e^4 + 292e^2 + 96)\eta v^9}{15M\epsilon^7} [1 + \beta_2 v^2 + \beta_3 v^3 + \beta_4 v^4 + \mathcal{O}(v^5)] \quad (9)$$

$$f_{22} = \frac{v^3}{\pi M} \quad (10)$$

where  $\epsilon = \sqrt{1 - e^2}$ , and  $\alpha_i, \beta_i$  are PN coefficients that depend on  $e$  and  $\eta$  [36, 66–69]<sup>3</sup>. For the purposes of this work, we will use equations accurate up to 2PN order (i.e. terms up to  $\mathcal{O}(v^4)$ ), and will neglect the effect of spin. We note that the full expressions are known up

to 3PN order [69] including the effect of spin [70], but we find that restricting to 2PN gives results accurate enough for our purposes. Evolving the above equations in time starting from the initial conditions, we extract eccentricities at an appropriate reference frequency. This way of defining eccentricity makes it consistent with the one defined in waveforms, modulo systematics in modeling the GW emission itself. In the next section, we compare estimates derived from the prescription mentioned above (which we denote by  $e_t^{2\text{PN}}$ ) to the those derived from the W03 prescription (denoted as  $e_{\text{W03}}$ ) as used in the astrophysical simulations literature, and also investigate potential biases due to incomplete physics.

<sup>2</sup> Beyond the drawbacks mentioned here, we also note that, on account of being orbit-averaged, the Peters equations break down when the orbital time scale  $\tau_{\text{orb}}$  is much greater than the radiation reaction time scale  $\tau_{\text{rr}}$  (e.g. at large separations and high eccentricity; see for instance the discussion in [65] and references therein.). However, since end states of binaries from typical simulations follow  $\tau_{\text{rr}} \gg \tau_{\text{orb}}$ , we do not attempt to account for this issue.

<sup>3</sup> See Appendix A for explicit expressions of these.

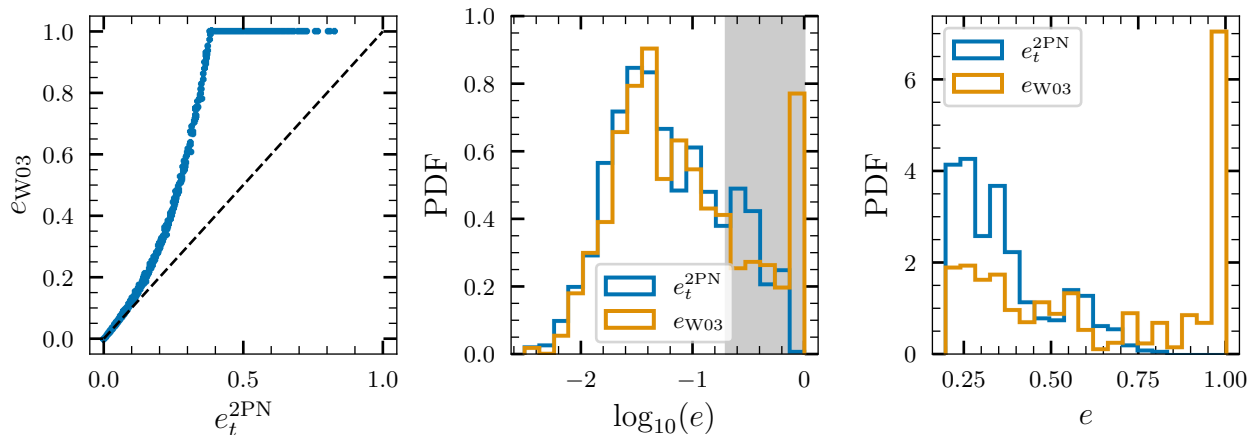


Figure 2. Comparison of orbital eccentricities in CMC simulations derived using the W03 prescription ( $e_{W03}$ ), to ones derived using the prescription in this work ( $e_t^{2PN}$ ). The left panel shows a scatter plot of the two quantities. We see that there is considerable disagreement on the derived values of eccentricity, especially at  $e \gtrsim 0.2$ . This can be understood as the effect of the peak frequencies being shifted to higher  $n_{\text{peak}}$ . The middle panel shows the histogram of (log) eccentricities for GW captures in globular clusters that occur during strong, few-body resonating interactions, derived using the W03 prescription and the prescription described in this work. The histograms do not deviate significantly from each other at low values of eccentricity, but are significantly different at  $e \gtrsim 0.2$  (shaded region). The right panel shows the histogram of eccentricities in this  $e \gtrsim 0.2$  region, where the discrepancies are more evident. Notably, the peak at  $e \approx 1$  is no longer present in the histogram; this peak is an artifact of the procedure used to extract eccentricity in astrophysical simulations.

### A. Comparison with the W03 prescription

As an illustration of our prescription, we consider binary mergers simulated with the Cluster Monte Carlo (CMC) code [71]. CMC performs long-term evolution of a globular cluster using a Hénon type Monte Carlo algorithm [72–81] given a set of initial conditions for the cluster. While we will only consider the CMC simulations as an example in this section, we again note that the W03 prescription has been in many other works (see e.g. [14, 16, 18, 25, 60, 61]).

A catalog of CMC simulations on a grid of initial cluster masses, metallicity, radii, and galactocentric distances is publicly available [82, 83]. This catalog also includes information about compact object mergers that take place in these clusters. Merging compact binaries are extracted from these simulations using the following procedure:

1. During strong GW encounters, the approximated  $N$ -body dynamics (including leading-order PN corrections that account for orbital energy dissipation from GW emission [84]) is evolved until two of the compact objects are in a bound state and reach a critical separation (typically  $100M$ ), at which point the binary is assumed to definitively lead to a GW-driven merger and the properties of the binary are recorded.
2. With this pair of eccentricity and semimajor axis, the eccentricity at a given reference frequency is extracted using the prescription of W03.

Instead of relying on the W03 definition of eccentricity, we apply the procedure outlined in Section III to each binary extracted from the simulations. We then calculate eccentricities at a fixed 22-mode reference frequency of 10 Hz. In the upper panel of Figure 2, we show a scatter plot of eccentricities derived from the two different definitions. Here,  $e_{W03}$  corresponds to the eccentricity as calculated by the W03 prescription, whereas  $e_t^{2PN}$  corresponds to the one calculated using the prescription presented in this work. At low eccentricities, the two definitions agree with each other. However, as one increases the eccentricity, the disagreement between the two increases quite rapidly. This is a direct result of the peak frequency getting shifted to higher harmonics as one increases eccentricity; for higher eccentricity, a given peak frequency  $f_{\text{peak,GW}}$  will correspond to a lower  $f_{22}$  (since  $\frac{1}{2}n_{\text{peak}}f_{22} = f_{\text{peak,GW}}$ ), hence describing the  $e_t^{2PN}$  at a much lower reference frequency. This also means that the binary will lose more of its eccentricity by the time it reaches  $f_{22} = 10$  Hz. As a consequence,  $e_t^{2PN}$  is always less than  $e_{W03}$ .

Notably, all the points that have  $e_{W03} \approx 1$  have  $e_t^{2PN}$  that range from 0.4 – 0.8. We note that in many places in the literature, this  $e \approx 1$  peak has been interpreted to be binaries that form “in-band” and merge quickly after getting captured; these are classically hyperbolic systems that are captured with a periaapse frequency *above* the reference frequency considered (e.g., 10 Hz) via orbital



energy loss through GW emission<sup>4</sup>. While that interpretation still remains qualitatively correct, our analysis shows that the value of eccentricity that should be supplied to waveforms in comparison studies is not  $e \approx 1$  but rather is shifted to much lower values.

The middle panel of Figure 2 shows histograms of  $e_{W03}$  and  $e_t^{2PN}$  calculated from the CMC simulations, with appropriate weights applied to each sample based on cluster mass, metallicity, and detection probability<sup>5</sup>. As would be expected from the preceding discussions, the histograms match for low values of eccentricity, and start deviating at  $e \gtrsim 0.2$ . Most strikingly, the peak at  $e_{W03} \approx 1$  in the  $e_{W03}$  histogram is not present in the  $e_t^{2PN}$  histogram. These observations are more evident in the right panel of Figure 2, where we show the histograms of eccentricities for  $e > 0.2$ . Since the waveform changes significantly as a function of eccentricity, one would expect these discrepancies to impact any analysis that assumes consistency between the definitions of eccentricities in waveforms and astrophysical simulations. We will comment on this briefly in Section III D.

In the preceding discussion, we have assumed that the reference frequency is defined in the source-frame of the binary as opposed to the detector-frame. We make this choice since the original calculation of eccentricity using the W03 prescription with the CMC outputs made this choice. Strictly, this is incorrect and adds another significant level of inconsistency in the conventions for eccentricity. For completeness, we also show the eccentricity extracted at a reference frequency corresponding to a constant  $f_{22}M = 1000 \text{ Hz}M_\odot$  in Figure 3, as  $f_{22}M$  does not depend on redshift. At a  $f_{22}$  corresponding to constant  $f_{22}M$ , all (black hole) binaries would be at the same epoch in their orbital evolution, i.e. they will all be at a fixed number of cycles before merger. This criterion is easy to implement while estimating parameters from BBH signals, and also allows for a more direct comparison of eccentricities for systems with different masses.

It is natural to ask whether the discrepancy is primarily driven by the mismatch in conventions for the reference frequency, or due to only accounting for the leading order PN term in the W03 prescription. The results in the preceding paragraphs would lead us to believe that it is the former. We test this in another way: since we know  $n_{\text{peak}}(e)$ , we can also adjust the eccentricities calculated via W03 as a post-processing step by assuming that the  $e_{W03}$  is defined at a reference frequency  $f_{22} = 2 \times f_{\text{peak}}/n_{\text{peak}}(e)$ , and evolve to a fixed reference (22-mode) frequency using PN equations (Eqs. (8)-(10))

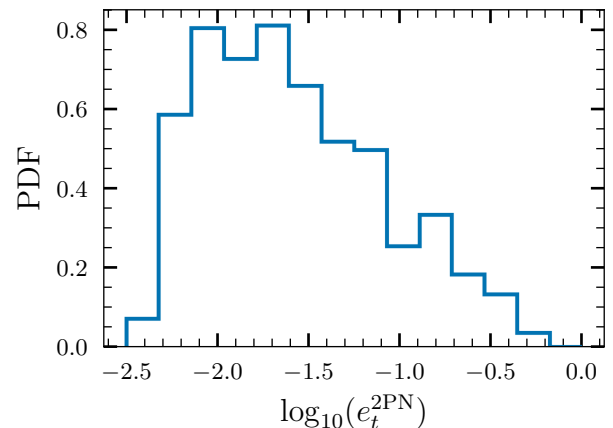


Figure 3. Histogram of eccentricities extracted at  $Mf_{22} = 1000 M_\odot \text{ Hz}$ . Defining the eccentricity at a fixed  $Mf_{22}$  has a few advantages: (i)  $Mf_{22}$  is independent of redshift, (ii) it defines eccentricity consistently at a fixed number of cycles before merger, and (iii) it is easy to implement while estimating source parameters from BBH signals. We recommend that all astrophysical simulations provide  $e_t^{2PN}$  estimates extracted at a fixed  $Mf_{22}$  for easy comparison with estimates of eccentricity derived using GW waveform models.

but only up to the leading order. Let the eccentricity calculated using this modified version of the W03 procedure be  $e_{W03}^{f_{22}}$ . We find that  $e_{W03}^{f_{22}} \approx e_t^{2PN}$  for the binaries we consider<sup>6</sup>, with a  $\sim 5\%$  scatter that could be attributed to non-inclusion of higher-order PN terms (see also Section III B). This further confirms that the discrepancy in the calculated eccentricities is primarily driven by the difference in conventions for the reference frequency.

### B. Effects of ignoring higher order PN terms and spin effects

We now systematically investigate if there is a relative advantage in using the 2PN equations above just the leading order (0PN) evolution equations. For an equal mass binary of total mass  $M = 50 M_\odot$ , we consider three different starting frequencies  $f_0 = 5, 10, 15 \text{ Hz}$ , and calculate  $e_t^{2PN}$  and  $e_t^{0PN}$  at a reference frequency of 20 Hz for a range of initial eccentricities  $e_0$ . The fractional differences between  $e_t^{2PN}$  and  $e_t^{0PN}$  estimates are plotted in the top panel of Figure 4, and show an increasing trend for lower values of  $f_0$ , with a discrepancy as high as 12% for  $f_0 = 5 \text{ Hz}$ . For a given  $f_0$ , the fractional differences are lower for higher  $e_0$ . In typical applications, one might want to calculate eccentricities at a given reference frequency for much lower values of  $f_0$ . While a  $\sim 10\%$

<sup>4</sup> We note that the  $e \approx 1$  value for systems in astrophysical simulations is somewhat artificial. These represent systems that do not have a defined eccentricity at a particular reference frequency according to the prescription outlined in Section II B and thus correspond to  $e \geq 1$  at a particular reference frequency.

<sup>5</sup> See e.g. Appendix A of Ref. [30] (and references therein) for a description of this weighting procedure.

<sup>6</sup> We exclude binaries with  $e_{W03} \approx 1$  from this calculation, due to their aforementioned artificial nature.

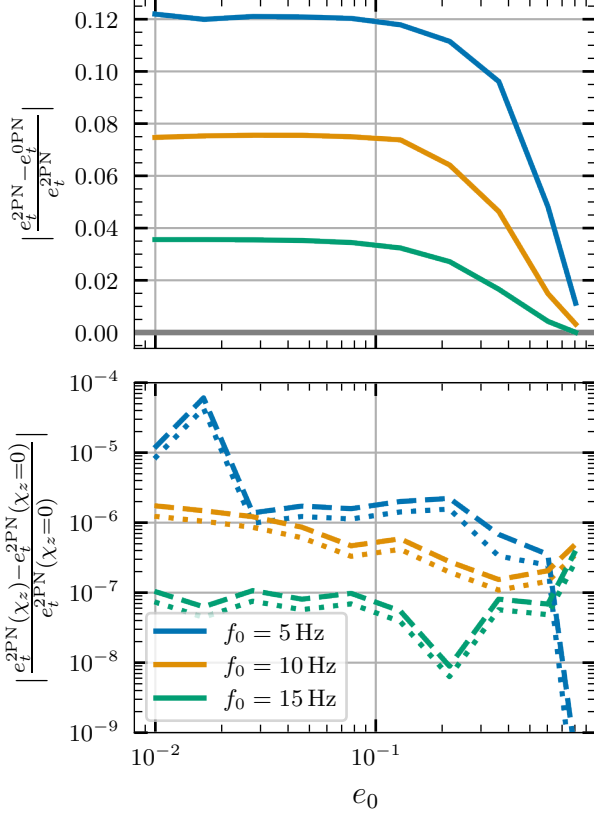


Figure 4. The top panel compares  $e_t^{0\text{PN}}$  and  $e_t^{2\text{PN}}$  computed at  $f_{\text{ref}} = 20$  Hz for three initial frequencies  $f_0 = 5, 10, 15$  Hz as a function of initial eccentricity  $e_0$ . The bottom panel makes a similar comparison between  $e_t^{2\text{PN}}$  calculated assuming a value  $\chi_z = \chi_{1,z} = \chi_{2,z}$ , and  $\chi_z = 0$ . We choose two representative values of  $\chi_z$ :  $\chi_z = 0.7$  (dotted lines), and  $\chi_z = 0.99$  (dashed lines).

difference might not be relevant while comparing eccentricity estimates from data to simulations, we recommend using  $e_t^{2\text{PN}}$  estimates since the costs of evaluating  $e_t^{0\text{PN}}$  and  $e_t^{2\text{PN}}$  are similar (see Appendix C).

Our prescription in Section III does not include the effects of spin. To see if this is a valid choice, we use the same mass,  $f_0$ ,  $f_{\text{ref}}$ , and  $e_0$  values as in the previous paragraph and calculate  $e_t^{2\text{PN}}$  with and without including spin terms in the evolution for two representative dimensionless (aligned) spin values of  $\chi_{1,z} = \chi_{2,z} = \chi_z = [0.7, 0.99]$ . For the spin terms in the evolution, we use 2PN accurate terms from Ref. [62]. The fractional differences between  $e_t^{2\text{PN}}$  estimates with and without spin effects are shown in the lower panel of Figure 4. We see that the discrepancies are at worst  $\sim 10^{-5}$ , shifting to even lower values when considering smaller fiducial spins or higher  $f_0$ . We hence conclude that the non-spinning approximation is sufficient.

### C. Comparison to estimates derived from gw\_eccentricity package

As mentioned earlier, different GW waveform approximants have different conventions to define eccentricity. To solve this issue, Ref. [57] proposed a standardized definition of eccentricity that can be applied to any waveform approximant,  $e_{\text{gw}}$ , which is given by

$$e_{\text{gw}} = \cos(\Psi/3) - \sqrt{3} \sin(\Psi/3), \quad (11)$$

where

$$\Psi = \arctan\left(\frac{1 - e_{\omega_{22}}^2}{2e_{\omega_{22}}}\right), \quad (12)$$

$$e_{\omega_{22}}(t) = \frac{\sqrt{\omega_{22}^{\text{p}}(t)} - \sqrt{\omega_{22}^{\text{a}}(t)}}{\sqrt{\omega_{22}^{\text{p}}(t)} + \sqrt{\omega_{22}^{\text{a}}(t)}}, \quad (13)$$

and  $\omega_{22}^{\text{p,a}}(t)$  are the 22-mode frequencies through the pericenters and apocenters, respectively. This standardized definition is proposed in order to extract eccentricity directly from observables, in this case the gravitational waveform. More details on the motivations for this definition and the various methods of calculating  $\omega_{22}^{\text{p,a}}(t)$  can be found in Ref. [57]. We also briefly investigate the differences between  $e_{\text{gw}}$  derived from different waveform approximants in Appendix B.

While  $e_{\text{gw}}$  does asymptote to the PN definition of eccentricity, these two definitions may differ in general. For instance, waveforms could include more accurate dynamics at high eccentricity and closer to merger as compared to our 2PN prescription. Instead of the 2PN accurate equations, we could hence imagine replacing the prescription in Section III by generating waveforms at the spec-

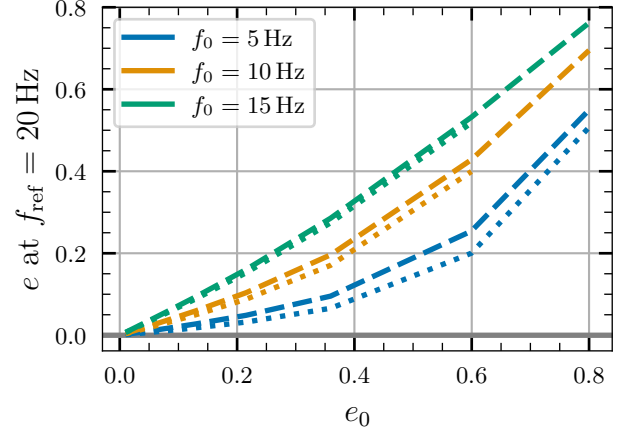


Figure 5. Comparison between the eccentricity definition given by Ref. [57], calculated using the waveform approximant SEOBNRv4EHM ( $e_{\text{gw}}^{\text{SEOB}}$ ; dotted lines), and  $e_t^{2\text{PN}}$  (dashed lines), as a function of the initial eccentricity,  $e_0$ , for three initial frequencies,  $f_0 = 5, 10, 15$  Hz. We assume an equal mass non-spinning binary with total mass  $M = 50 M_{\odot}$  for this purpose.

ified initial epochs, and let `gw_eccentricity` calculate the eccentricities at the required reference frequency.

However, since calculating  $e_{\text{gw}}$  involves computing the waveform starting at a specified initial frequency/time, the calculation would be on the order of a hundred times slower (see Appendix C) than computing the PN eccentricity. The cost of generating waveforms also increases with decreasing starting frequency. Since astrophysical simulations require calculating eccentricities of a large number of binaries, calculating the Ref. [57] definition of eccentricity would be computationally inefficient. Therefore, we now compare the differences between the two eccentricity definitions,  $e_{\text{gw}}$  and  $e_t^{2\text{PN}}$ , and quantify the reliability of  $e_t^{2\text{PN}}$  eccentricity estimates from astrophysical simulations. For the investigations that follow, we will use the SEOBNRv4EHM [48] waveform approximant for the calculation of  $e_{\text{gw}}$ . Using the same mass,  $f_0$ , and  $e_0$  values as in Section III B, we calculate  $e_t^{2\text{PN}}$  and  $e_{\text{gw}}^{\text{SEOB}}$  at a reference frequency of 20 Hz. Figure 5 illustrates the differences between these. While small (a few tens of a percent at worst), the differences do accumulate as the binary evolves for a longer period of time with  $f_0$  values closer to the reference frequency giving more agreement. Since the cost of computing  $e_{\text{gw}}$  is a factor of  $\sim 100$  greater as compared to calculating  $e_t^{2\text{PN}}$  (see Appendix C), we conclude that  $e_t^{2\text{PN}}$  is sufficient, especially in regimes where PN theory is valid.

#### D. Implications for existing work

A number of works have ascertained the detectability of eccentric mergers within the LVK band as well as in other detector bands, using data from astrophysical simulations such as CMC. As we have shown in the previous sections, the waveform eccentricities are not in agreement with the eccentricities given by simulations. Hence, we would expect these detectability estimates to change when defining eccentricity consistently in the simulations. For instance, Ref. [30] found that  $\approx 60\%$  of potentially detectable eccentric sources with  $e \gtrsim 0.2$  would be missed due to non-inclusion of eccentric templates in search pipelines. Using the same dataset as Ref. [30] and changing the eccentricities from the  $e_{\text{W03}}$  definition to the  $e_t^{2\text{PN}}$  definition, we find that only 30% of potentially detectable eccentric sources with  $e \gtrsim 0.2$  are missed—a discrepancy by a factor of  $\approx 2$ . The decrease in the number of missed signals is due to the shifting of the histogram of eccentricities towards lower values, which are better approximated by non-eccentric templates and hence less likely to be selected against. As another illustration, we calculate limits on the cluster branching fraction  $\beta_c$  i.e the fraction of events in the total population coming from clusters using the same method and dataset as used in Ref. [8]. We find that assuming  $N_{\text{ecc}} = 0$  eccentric detections in GWTC-3, we would have inferred  $\beta_c < 86\%$  (90% credible level) using the  $e_{\text{W03}}$  estimates, and infer  $\beta_c < 63\%$  using the  $e_t^{2\text{PN}}$  estimates. On the other

hand, assuming  $N_{\text{ecc}} = 1$  gives  $\beta_c > 10\%$  using the  $e_{\text{W03}}$  estimates and  $\beta_c > 8\%$  using the  $e_t^{2\text{PN}}$  estimates.

Similarly, any study that uses the detected eccentricities (or lack thereof) to place constraints on the overall merger rate in eccentric systems in astrophysical environments will also be affected by these discrepancies. For instance, Ref. [44] use the non-detection of orbital eccentricity from a waveform-independent search to place an upper limit of  $0.34 \text{ Gpc}^{-3} \text{ yr}^{-1}$  on the merger rate of binaries in dense stellar clusters, assuming a population model from CMC simulations. This population model is taken from Ref. [30] with eccentricities defined using the W03 prescription, with additional conditioning on the mass ( $M > 70$ ) and eccentricity ( $e < 0.3$ ) parameter ranges of their search. From Figure 2, we see that the relative number of mergers having  $e < 0.3$  increases when accounting for the prescription in this work. This means that an upper limit derived using the  $e_t^{2\text{PN}}$  estimates from this work would be lower than the ones quoted in Ref. [44].

We also note that Ref. [85], which uses signatures of non-zero eccentricity in four GW events to constrain the fraction of BBH mergers formed dynamically, does account for the disparate conventions for eccentricity while making their comparisons. They do so in an approximate fashion, similar to the calculation of  $e_{\text{W03}}^{f_{22}}$  described in Section III A. We do not expect conclusions reported there to change significantly.

#### IV. CONCLUSION

Orbital eccentricity in a compact binary is believed to be a telltale sign of its formation history. Consequently, there has been progress on building waveform models for eccentric sources as well as on simulating expectations from astrophysical formation channels. In this work, we note that the conventions used to define eccentricity in the GW waveform and astrophysical simulation communities differ from each other. The major difference in these conventions lies in the choice of the reference frequency at which eccentricity is defined—GW waveforms typically define eccentricity at a fixed orbit averaged 22-mode GW frequency, while astrophysical simulations define eccentricity at a fixed peak GW frequency following the W03 prescription (described in Section II B). Further, we delineate an eccentricity calculation procedure that can be applied to data from astrophysical simulations to extract eccentricities consistent with conventions laid down by the GW waveform community. This procedure involves evolution of ordinary differential equations describing the time-evolution of eccentricity and frequency obtained from PN expansions, and extracting eccentricity consistently at the orbit-averaged 22 mode frequency.

Using compact binaries from the publicly-available CMC catalog as an illustration, we find that there is a discrepancy between eccentricity estimates derived using the W03 prescription and the one described in this work. The discrepancy is small for  $e \lesssim 0.1$ , but is large



for higher values of eccentricity. Notably, all binaries with  $e_{W03} \approx 1$  (thought to be GW captures happening in the LVK band) have  $e_t^{2PN}$  between 0.4–0.8. We investigate the effect that adding 2PN corrections to the leading order evolution has on derived eccentricities, and also the effects of not including spins in our prescription. We also compare our  $e_t^{2PN}$  estimates to  $e_{gw}$  estimates derived from the `gw_eccentricity` package using the `SEOBNRv4EHM` waveform. We find that the  $e_t^{2PN}$  estimates should be sufficiently accurate in extracting eccentricities, and also computationally efficient to implement as a post-processing step in simulations. However, as outlined in Ref. [57], `gw_eccentricity` is the most accurate way of extracting eccentricity and should be used when high-precision eccentricity estimates are necessary.

The different conventions for defining eccentricity currently employed in the literature mean that one should be careful in comparing eccentricity estimates/upper limits derived from real data to astrophysical simulations, creating mock populations of eccentric sources based on astrophysical expectations, and other investigations that pair predictions from astrophysical models with GW data analysis. As an illustration, we show that the detectability estimates of eccentric sources and branching fractions from Ref. [30] will change when ensuring a consistent definition of eccentricity. We recommend that catalogs created from astrophysical simulations include  $e_t^{2PN}$  estimates (extracted at a constant  $Mf_{22}$ ) for clarity and ease of direct comparison to GW observations.

## ACKNOWLEDGEMENTS

We are grateful to Isobel Romero-Shaw for a thorough reading of our draft and useful suggestions. We thank Kaushik Paul for insightful inputs regarding PN equations and sharing code for the same, and Antoni Ramos-Buades for providing access to the `SEOBNRv4EHM` approximant. We also thank Vijay Varma, Prayush Kumar, Bala Iyer, and Akash Maurya for useful discussions. Example python scripts are available at <https://github.com/advijaykumar/standard-eccentricity-scripts>, and data products are available on Zenodo [58].

AV is supported by the Natural Sciences and Engineering Research Council of Canada (NSERC) (funding reference number 568580), and the Department of Atomic Energy, Government of India, under Project No. RTI4001. AV also acknowledges support by a Fulbright Program grant under the Fulbright-Nehru Doctoral Research Fellowship, sponsored by the Bureau of Educational and Cultural Affairs of the United States Department of State and administered by the Institute of International Education and the United States-India Educational Foundation. AGH is supported by NSF grants AST-2006645 and PHY2110507. AGH gratefully acknowledges the ARCS Foundation Scholar Award through the ARCS Foundation, Illinois Chapter with support from the Brinson Founda-

tion. MZ gratefully acknowledges funding from the Brinson Foundation in support of astrophysics research at the Adler Planetarium. This work has made use of the `numpy` [86], `scipy` [87], `matplotlib` [88], `astropy` [89, 90], `jupyter` [91], `pandas` [92], `seaborn` [93], and `lalsuite` [94] software packages.

## Appendix A: PN formulae for eccentricity and velocity evolution

The PN formulae (accurate up to 2PN) for the evolution of eccentricity and velocity are given below

$$\frac{de}{dt} = -\frac{e(121e^2 + 304)\eta v^8}{15M\epsilon^5} [1 + \alpha_2 v^2 + \alpha_3 v^3 + \alpha_4 v^4 + \mathcal{O}(v^5)] \quad (\text{A1})$$

$$\frac{dv}{dt} = \frac{(37e^4 + 292e^2 + 96)\eta v^9}{15M\epsilon^7} [1 + \beta_2 v^2 + \beta_3 v^3 + \beta_4 v^4 + \mathcal{O}(v^5)] \quad (\text{A2})$$

$$f_{22} = \frac{v^3}{\pi M} \quad (\text{A3})$$

where

$$\alpha_2 = \frac{125361e^4 + 718008e^2 - 28(3328e^4 + 23259e^2 + 8168)\eta - 67608}{168(121e + 304)\epsilon^2} \quad (\text{A4})$$

$$\alpha_3 = \frac{1970\pi v^3 \epsilon^5}{121e + 304} \phi_e^{\text{rad}} \quad (\text{A5})$$

$$\begin{aligned} \alpha_4 = & \frac{1}{2016(121e + 304)\epsilon^4} [3e^6 (919520\eta^2 - 1448284\eta + 1262181) \\ & + e^4 (42810096\eta^2 - 78343602\eta - 569520(2\eta - 5)\epsilon + 46566110) \\ & - 12e^2 (3495771\eta + 584892(2\eta - 5)\epsilon - 945290) \\ & - 16 (-284256\eta^2 - 801495\eta + 168336(2\eta - 5)\epsilon + 952397)] \end{aligned} \quad (\text{A6})$$

and

$$\beta_2 = \frac{e^6(11717 - 8288\eta) + e^4(171038 - 141708\eta) - 120e^2(1330\eta - 731) + 16(743 - 924\eta)}{56(37e^4 + 292e^2 + 96)\epsilon^2} \quad (\text{A7})$$

$$\beta_3 = \frac{768\pi v^3 \epsilon^7}{74e^4 + 584e^2 + 192} \phi_e \quad (\text{A8})$$

$$\begin{aligned} \beta_4 = & -\frac{1}{6048(37e^4 + 292e^2 + 96)\epsilon^4} [-3e^8 (654752\eta^2 - 1086660\eta + 1174371) \\ & + 6e^6 (-10804808\eta^2 + 20518071\eta + 88200(2\eta - 5)\epsilon - 13904067) \\ & + 12e^4 (-13875505\eta^2 + 17267022\eta + 1105272(2\eta - 5)\epsilon - 65314) \\ & + 16e^2 (-3830127\eta^2 - 966546\eta + 806652(2\eta - 5)\epsilon + 5802910) \\ & + 32 (-59472\eta^2 - 141093\eta + 9072(2\eta - 5)\epsilon + 11257)] \end{aligned} \quad (\text{A9})$$

Here,  $\epsilon = \sqrt{1 - e^2}$ . Here, the “enhancement factors”  $\phi_e$ ,  $\tilde{\phi}_e$ , and  $\phi_e^{\text{rad}}$  are given by

$$\phi_e = \frac{\frac{428340e^{12}}{9958749469} - \frac{5034498e^{10}}{7491716851} + \frac{9293260e^8}{3542508891} + \frac{48176523e^6}{177473701} + \frac{157473274e^4}{30734301} + \frac{18970894028e^2}{2649026657} + 1}{\epsilon^{10}} \quad (\text{A10})$$

$$\tilde{\phi}_e = \frac{-\frac{328675e^{10}}{8674876481} - \frac{4679700e^8}{6316712563} - \frac{2640201e^6}{993226448} + \frac{37570495e^4}{98143337} + \frac{413137256e^2}{136292703} + 1}{\epsilon^9} \quad (\text{A11})$$

$$\phi_e^{\text{rad}} = \frac{192\epsilon(\epsilon\phi_e - \tilde{\phi}_e)}{985e^2} \quad (\text{A12})$$

## Appendix B: Variation in gw\_eccentricity estimates calculated from different waveform approximants

The prescription of calculating eccentricity  $e_{\text{gw}}$ , proposed by [57] and implemented in the `gw_eccentricity` python package only uses the GW waveform as seen by the detector as input, as described in Section III C. This definition is beneficial since eccentricity is now linked to a direct observable. However, different waveforms will, in general, yield different values of  $e_{\text{gw}}$  for the same binary. This could be due to a variety of reasons: differences in the modeling of the dynamics, different internal definitions of eccentricity in the model, or even choices made while implementing the

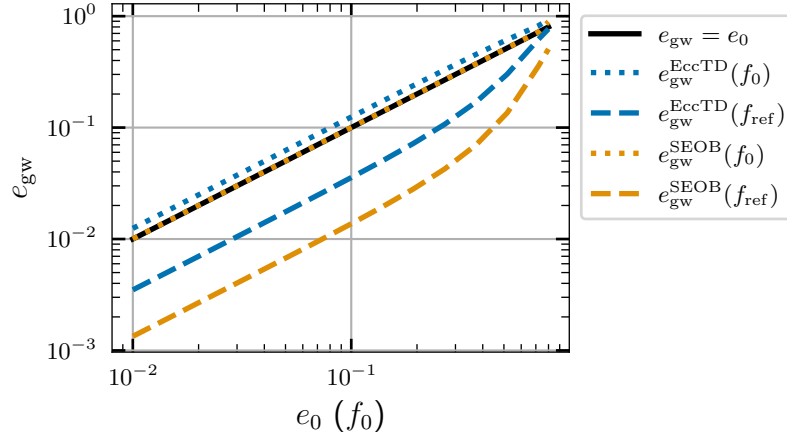


Figure 6. Comparison of internal definitions of eccentricity for different waveform models as a function of the initial input eccentricity,  $e_0$  with a fiducial input frequency of 5 Hz. Initial eccentricities using the standardized definition,  $e_{\text{gw}}(f_0)$  (dotted lines), should be consistent with the input eccentricity  $e_0$  (black line). **EccentricTD** (blue) does not agree for any value of  $e_0$ , while **SEOBNRv4EHM** (yellow) does agree for all  $e_0$  values considered. We also see that the final eccentricity reported for the given reference frequency  $f_{\text{ref}}$  between the two waveforms (blue and yellow dashed lines) do not agree.

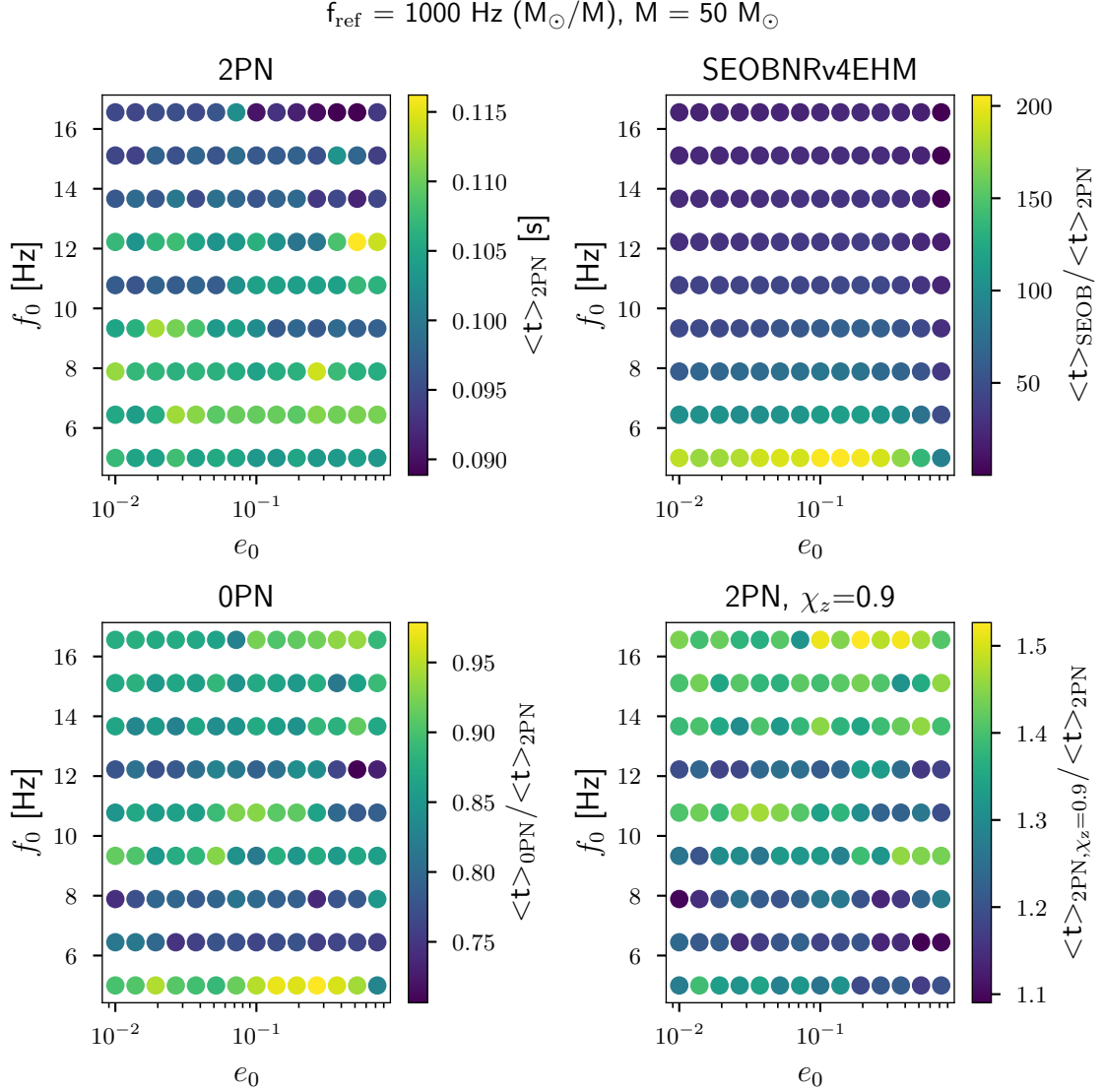
approximant in some codebase such as **LALSimulation** [94]. Figure 6 illustrates this point by comparing  $e_{\text{gw}}$  derived from two waveforms, **EccentricTD** [45] and **SEOBNRv4EHM** [48]. For this illustration, we assume an equal mass binary with a total mass of  $M = 50 M_\odot$ . We vary the initial eccentricity  $e_0$  (defined at initial frequency  $f_0 = 5$  Hz) supplied to the model between  $10^{-2}$  and 0.8, and extract  $e_{\text{gw}}$  from both **EccentricTD** ( $e_{\text{gw}}^{\text{EccTD}}$ ) and **SEOBNRv4EHM** ( $e_{\text{gw}}^{\text{SEOB}}$ ), at both the initial frequency  $f_0$  and also at  $f_{\text{ref}} = 20$  Hz. We see that  $e_{\text{gw}}^{\text{SEOB}}(f_0)$  matches all input values  $e_0$ , whereas  $e_{\text{gw}}^{\text{EccTD}}(f_0)$  differs from  $e_0$  by a few percent. This is in agreement with investigations performed in Ref. [57], where they found that the  $e_{\text{gw}}^{\text{SEOB}}(f_0) = e_0$  trend is maintained for all  $e_0 > 10^{-5}$ , whereas  $e_{\text{gw}}^{\text{EccTD}}$  deviates from the  $e_{\text{gw}}^{\text{EccTD}}(f_0) = e_0$  trend. We also see that there is a large discrepancy (factor of a few) between  $e_{\text{gw}}^{\text{EccTD}}(f_{\text{ref}})$  and  $e_{\text{gw}}^{\text{SEOB}}(f_{\text{ref}})$ , strengthening the evidence for differences in the ways each of these waveform approximants define eccentricity. We use the **SEOBNRv4EHM** approximant for our comparisons in Section III C.

### Appendix C: Computational cost of different eccentricity prescriptions

Astrophysical simulations keep track of many evolving binary systems, where it is often computationally infeasible to compute waveforms for all systems. In Figure 7, we demonstrate the speed-up in eccentricity calculation at the reference frequency,  $f_{\text{ref}}$ , by computing the PN eccentricities,  $e_t^{k\text{PN}}$ , as opposed to the standardized waveform definition of eccentricity,  $e_{\text{gw}}$ . The top left of Figure 7 demonstrates the average time to compute the 2PN eccentricity at various initial eccentricities,  $e_0$ , and frequencies,  $f_0$ . The top right plot illustrates that computing the waveform eccentricity,  $e_{\text{gw}}$  using the **SEOBNRv4EHM** waveform model takes on the order of a hundred times longer on average. The bottom plots in Figure 7 demonstrate that using the 0PN eccentricity has a comparable cost to using the 2PN eccentricity, whereas including spin effects in the PN equations is  $\sim 1.5$  times slower.

### REFERENCES

- 
- [1] LIGO Scientific Collaboration, J. Aasi, B. P. Abbott, R. Abbott, T. Abbott, M. R. Abernathy, K. Ackley, C. Adams, T. Adams, P. Addesso, *et al.*, “Advanced LIGO,” *Classical and Quantum Gravity* **32**, 074001 (2015), arXiv:1411.4547 [gr-qc].
  - [2] F. Acernese, M. Agathos, K. Agatsuma, D. Aisa, N. Allemandou, A. Allocca, J. Amarni, P. Astone, G. Balestri, G. Ballardin, *et al.*, “Advanced Virgo: a second-generation interferometric gravitational wave detector,” *Classical and Quantum Gravity* **32**, 024001 (2015), arXiv:1408.3978 [gr-qc].
  - [3] Yoichi Aso, Yuta Michimura, Kentaro Somiya, Masaki Ando, Osamu Miyakawa, Takanori Sekiguchi, Daisuke Tatsumi, and Hiroaki Yamamoto, “Interferometer design



of the KAGRA gravitational wave detector,” *Phys. Rev. D* **88**, 043007 (2013), [arXiv:1306.6747 \[gr-qc\]](#).

- [4] T. Akutsu, M. Ando, K. Arai, Y. Arai, S. Araki, A. Araya, N. Aritomi, Y. Aso, S. Bae, Y. Bae, L. Baiotti, R. Bajpai, M. A. Barton, K. Cannon, E. Capocasa, M. Chan, C. Chen, K. Chen, Y. Chen, H. Chu, Y. K. Chu, S. Eguchi, Y. Enomoto, R. Flaminio, Y. Fujii, M. Fukushima, M. Fukushima, G. Ge, A. Hagiwara, S. Haino, K. Hasegawa, H. Hayakawa, K. Hayama, Y. Himemoto, Y. Hiranuma, N. Hirata, E. Hirose, Z. Hong, B. H. Hsieh, C. Z. Huang, P. Huang, Y. Huang, B. Ikenoue, S. Imam, K. Inayoshi, Y. Inoue, K. Ioka, Y. Itoh, K. Izumi, K. Jung, P. Jung, T. Kajita, M. Kamizumi, N. Kanda, G. Kang, K. Kawaguchi, N. Kawai, T. Kawasaki, C. Kim, J. C. Kim, W. S. Kim, Y. M.

Kim, N. Kimura, N. Kita, H. Kitazawa, Y. Kojima, K. Kokeyama, K. Komori, A. K. H. Kong, K. Kotake, C. Kozakai, R. Kozu, R. Kumar, J. Kume, C. Kuo, H. S. Kuo, S. Kuroyanagi, K. Kusayanagi, K. Kwak, H. K. Lee, H. W. Lee, R. Lee, M. Leonardi, L. C. C. Lin, C. Y. Lin, F. L. Lin, G. C. Liu, L. W. Luo, M. Marchio, Y. Michimura, N. Mio, O. Miyakawa, A. Miyamoto, Y. Miyazaki, K. Miyo, S. Miyoki, S. Morisaki, Y. Moriwaki, K. Nagano, S. Nagano, K. Nakamura, H. Nakano, M. Nakano, R. Nakashima, T. Narikawa, R. Negishi, W. T. Ni, A. Nishizawa, Y. Obuchi, W. Ogaki, J. J. Oh, S. H. Oh, M. Ohashi, N. Ohishi, M. Ohkawa, K. Okutomi, K. Oohara, C. P. Ooi, S. Oshino, K. Pan, H. Pang, J. Park, F. E. Peña Arellano, I. Pinto, N. Sago, S. Saito, Y. Saito, K. Sakai, Y. Sakai, Y. Sakuno, S. Sato,



- T. Sato, T. Sawada, T. Sekiguchi, Y. Sekiguchi, S. Shibagaki, R. Shimizu, T. Shimoda, K. Shimode, H. Shinkai, T. Shishido, A. Shoda, K. Somiya, E. J. Son, H. Sotani, R. Sugimoto, T. Suzuki, T. Suzuki, H. Tagoshi, H. Takahashi, R. Takahashi, A. Takamori, S. Takano, H. Takeda, M. Takeda, H. Tanaka, K. Tanaka, K. Tanaka, T. Tanaka, T. Tanaka, S. Tanioka, E. N. Tapia San Martin, S. Telada, T. Tomaru, Y. Tomigami, T. Tomura, F. Travasso, L. Trozzo, T. Tsang, K. Tsubono, S. Tsuchida, T. Tsuzuki, D. Tuyenbayev, N. Uchikata, T. Uchiyama, A. Ueda, T. Uehara, K. Ueno, G. Ueshima, F. Uraguchi, T. Ushiba, M. H. P. M. van Putten, H. Vocca, J. Wang, C. Wu, H. Wu, S. Wu, W. R. Xu, T. Yamada, K. Yamamoto, K. Yamamoto, T. Yamamoto, K. Yokogawa, J. Yokoyama, T. Yokozawa, T. Yoshioka, H. Yuzurihara, S. Zeidler, Y. Zhao, and Z. H. Zhu, “Overview of KAGRA: Detector design and construction history,” *Progress of Theoretical and Experimental Physics* **2021**, 05A101 (2021), [arXiv:2005.05574 \[physics.ins-det\]](#).
- [5] B. P. Abbott, R. Abbott, T. D. Abbott, M. R. Abernathy, F. Acernese, K. Ackley, C. Adams, T. Adams, P. Addesso, R. X. Adhikari, *et al.*, “Prospects for observing and localizing gravitational-wave transients with Advanced LIGO, Advanced Virgo and KAGRA,” *Living Reviews in Relativity* **21**, 3 (2018), [arXiv:1304.0670 \[gr-qc\]](#).
- [6] R. Abbott, T. D. Abbott, F. Acernese, K. Ackley, C. Adams, N. Adhikari, R. X. Adhikari, V. B. Adya, C. Affeldt, D. Agarwal, *et al.*, “GWTC-3: Compact Binary Coalescences Observed by LIGO and Virgo during the Second Part of the Third Observing Run,” *Physical Review X* **13**, 041039 (2023), [arXiv:2111.03606 \[gr-qc\]](#).
- [7] R. Abbott, T. D. Abbott, F. Acernese, K. Ackley, C. Adams, N. Adhikari, R. X. Adhikari, V. B. Adya, C. Affeldt, D. Agarwal, M. Agathos, K. Agatsuma, N. Aggarwal, O. D. Aguiar, L. Aiello, A. Ain, P. Ajith, T. Akutsu, P. F. de Alarcón, S. Akcay, S. Albanesi, A. Allocca, P. A. Altin, A. Amato, C. Anand, S. Anand, A. Ananyeva, S. B. Anderson, W. G. Anderson, M. Ando, T. Andrade, N. Andres, T. Andrić, S. V. Angelova, S. Ansoldi, J. M. Antelis, S. Antier, F. Antonini, S. Appert, Koji Arai, Koya Arai, Y. Arai, S. Araki, A. Araya, M. C. Araya, LIGO Scientific Collaboration, VIRGO Collaboration, and KAGRA Collaboration, “Population of Merging Compact Binaries Inferred Using Gravitational Waves through GWTC-3,” *Physical Review X* **13**, 011048 (2023), [arXiv:2111.03634 \[astro-ph.HE\]](#).
- [8] Michael Zevin, Simone S. Bavera, Christopher P. L. Berry, Vicky Kalogera, Tassos Fragos, Pablo Marchant, Carl L. Rodriguez, Fabio Antonini, Daniel E. Holz, and Chris Pankow, “One Channel to Rule Them All? Constraining the Origins of Binary Black Holes Using Multiple Formation Pathways,” *ApJ* **910**, 152 (2021), [arXiv:2011.10057 \[astro-ph.HE\]](#).
- [9] April Qiu Cheng, Michael Zevin, and Salvatore Vitale, “What You Don’t Know Can Hurt You: Use and Abuse of Astrophysical Models in Gravitational-wave Population Analyses,” *ApJ* **955**, 127 (2023), [arXiv:2307.03129 \[astro-ph.HE\]](#).
- [10] Ryan M. O’Leary, Bence Kocsis, and Abraham Loeb, “Gravitational waves from scattering of stellar-mass black holes in galactic nuclei,” *MNRAS* **395**, 2127–2146 (2009), [arXiv:0807.2638 \[astro-ph\]](#).
- [11] Bence Kocsis and Janna Levin, “Repeated bursts from relativistic scattering of compact objects in galactic nuclei,” *Phys. Rev. D* **85**, 123005 (2012), [arXiv:1109.4170 \[astro-ph.CO\]](#).
- [12] Johan Samsing, Morgan MacLeod, and Enrico Ramirez-Ruiz, “The Formation of Eccentric Compact Binary Inspirals and the Role of Gravitational Wave Emission in Binary-Single Stellar Encounters,” *ApJ* **784**, 71 (2014), [arXiv:1308.2964 \[astro-ph.HE\]](#).
- [13] Fabio Antonini, Silvia Toonen, and Adrian S. Hamers, “Binary Black Hole Mergers from Field Triples: Properties, Rates, and the Impact of Stellar Evolution,” *ApJ* **841**, 77 (2017), [arXiv:1703.06614 \[astro-ph.GA\]](#).
- [14] Johan Samsing and Enrico Ramirez-Ruiz, “On the Assembly Rate of Highly Eccentric Binary Black Hole Mergers,” *ApJ* **840**, L14 (2017), [arXiv:1703.09703 \[astro-ph.HE\]](#).
- [15] Kedron Silsbee and Scott Tremaine, “Lidov-Kozai Cycles with Gravitational Radiation: Merging Black Holes in Isolated Triple Systems,” *ApJ* **836**, 39 (2017), [arXiv:1608.07642 \[astro-ph.HE\]](#).
- [16] Carl L. Rodriguez, Pau Amaro-Seoane, Sourav Chatterjee, Kyle Kremer, Frederic A. Rasio, Johan Samsing, Claire S. Ye, and Michael Zevin, “Post-Newtonian dynamics in dense star clusters: Formation, masses, and merger rates of highly-eccentric black hole binaries,” *Phys. Rev. D* **98**, 123005 (2018), [arXiv:1811.04926 \[astro-ph.HE\]](#).
- [17] Carl L. Rodriguez and Fabio Antonini, “A Triple Origin for the Heavy and Low-spin Binary Black Holes Detected by LIGO/VIRGO,” *ApJ* **863**, 7 (2018), [arXiv:1805.08212 \[astro-ph.HE\]](#).
- [18] Johan Samsing, “Eccentric black hole mergers forming in globular clusters,” *Phys. Rev. D* **97**, 103014 (2018), [arXiv:1711.07452 \[astro-ph.HE\]](#).
- [19] Johan Samsing, Abbas Askar, and Mirek Giersz, “MOCCA-SURVEY Database. I. Eccentric Black Hole Mergers during Binary-Single Interactions in Globular Clusters,” *ApJ* **855**, 124 (2018), [arXiv:1712.06186 \[astro-ph.HE\]](#).
- [20] Johan Samsing, Daniel J. D’Orazio, Abbas Askar, and Mirek Giersz, “Black Hole Mergers from Globular Clusters Observable by LISA and LIGO: Results from post-Newtonian Binary-Single Scatterings,” *arXiv e-prints*, [arXiv:1802.08654 \(2018\)](#), [arXiv:1802.08654 \[astro-ph.HE\]](#).
- [21] Giacomo Fragione and Bence Kocsis, “Black hole mergers from quadruples,” *MNRAS* **486**, 4781–4789 (2019), [arXiv:1903.03112 \[astro-ph.GA\]](#).
- [22] Giacomo Fragione and Omer Bromberg, “Eccentric binary black hole mergers in globular clusters hosting intermediate-mass black holes,” *MNRAS* **488**, 4370–4377 (2019), [arXiv:1903.09659 \[astro-ph.GA\]](#).
- [23] Bin Liu, Dong Lai, and Yi-Han Wang, “Black Hole and Neutron Star Binary Mergers in Triple Systems. II. Merger Eccentricity and Spin-Orbit Misalignment,” *ApJ* **881**, 41 (2019), [arXiv:1905.00427 \[astro-ph.HE\]](#).
- [24] Bin Liu and Dong Lai, “Enhanced black hole mergers in binary-binary interactions,” *MNRAS* **483**, 4060–4069 (2019), [arXiv:1809.07767 \[astro-ph.HE\]](#).
- [25] Michael Zevin, Johan Samsing, Carl Rodriguez, Carl Johan Haster, and Enrico Ramirez-Ruiz, “Eccentric Black Hole Mergers in Dense Star Clusters: The Role of Binary-Binary Encounters,” *ApJ* **871**, 91 (2019), [arXiv:1810.00901 \[astro-ph.HE\]](#).
- [26] Erez Michaely and Hagai B. Perets, “High rate of gravitational waves mergers from flyby perturbations of wide black hole triples in the field,” *MNRAS* **498**, 4924–4935 (2020), [arXiv:2008.01094 \[astro-ph.HE\]](#).

- [27] László Gondán and Bence Kocsis, “High eccentricities and high masses characterize gravitational-wave captures in galactic nuclei as seen by Earth-based detectors,” *MNRAS* **506**, 1665–1696 (2021), [arXiv:2011.02507 \[astro-ph.HE\]](#).
- [28] Hiromichi Tagawa, Bence Kocsis, Zoltán Haiman, Imre Bartos, Kazuyuki Omukai, and Johan Samsing, “Eccentric Black Hole Mergers in Active Galactic Nuclei,” *ApJ* **907**, L20 (2021), [arXiv:2010.10526 \[astro-ph.HE\]](#).
- [29] Michela Mapelli, Marco Dall’Amico, Yann Bouffanais, Nicola Giacobbo, Manuel Arca Sedda, M. Celeste Artale, Alessandro Ballone, Ugo N. Di Carlo, Giuliano Iorio, Filippo Santoliquido, and Stefano Torniamenti, “Hierarchical black hole mergers in young, globular and nuclear star clusters: the effect of metallicity, spin and cluster properties,” *MNRAS* **505**, 339–358 (2021), [arXiv:2103.05016 \[astro-ph.HE\]](#).
- [30] Michael Zevin, Isobel M. Romero-Shaw, Kyle Kremer, Eric Thrane, and Paul D. Lasky, “Implications of Eccentric Observations on Binary Black Hole Formation Channels,” *ApJ* **921**, L43 (2021), [arXiv:2106.09042 \[astro-ph.HE\]](#).
- [31] Fupeng Zhang, Xian Chen, Lijing Shao, and Kohei Inayoshi, “The Eccentric and Accelerating Stellar Binary Black Hole Mergers in Galactic Nuclei: Observing in Ground and Space Gravitational-wave Observatories,” *ApJ* **923**, 139 (2021), [arXiv:2109.14842 \[astro-ph.HE\]](#).
- [32] J. Samsing, I. Bartos, D. J. D’Orazio, Z. Haiman, B. Kocsis, N. W. C. Leigh, B. Liu, M. E. Pessah, and H. Tagawa, “AGN as potential factories for eccentric black hole mergers,” *Nature* **603**, 237–240 (2022), [arXiv:2010.09765 \[astro-ph.HE\]](#).
- [33] Alessandro A. Trani, Sara Rastello, Ugo N. Di Carlo, Filippo Santoliquido, Ataru Tanikawa, and Michela Mapelli, “Compact object mergers in hierarchical triples from low-mass young star clusters,” *MNRAS* **511**, 1362–1372 (2022), [arXiv:2111.06388 \[astro-ph.HE\]](#).
- [34] Marco Dall’Amico, Michela Mapelli, Stefano Torniamenti, and Manuel Arca Sedda, “Eccentric black hole mergers via three-body interactions in young, globular and nuclear star clusters,” *arXiv e-prints*, [arXiv:2303.07421 \(2023\)](#), [arXiv:2303.07421 \[astro-ph.HE\]](#).
- [35] Isobel Romero-Shaw, Nicholas Loutrel, and Michael Zevin, “Inferring interference: Identifying a perturbing tertiary with eccentric gravitational wave burst timing,” *Phys. Rev. D* **107**, 122001 (2023), [arXiv:2211.07278 \[gr-qc\]](#).
- [36] P. C. Peters, “Gravitational Radiation and the Motion of Two Point Masses,” *Physical Review* **136**, 1224–1232 (1964).
- [37] H. von Zeipel, “Sur l’application des séries de M. Lindstedt à l’étude du mouvement des comètes périodiques,” *Astronomische Nachrichten* **183**, 345 (1910).
- [38] M.L. Lidov, “The evolution of orbits of artificial satellites of planets under the action of gravitational perturbations of external bodies,” *Planetary and Space Science* **9**, 719–759 (1962).
- [39] Yoshihide Kozai, “Secular perturbations of asteroids with high inclination and eccentricity,” *AJ* **67**, 591–598 (1962).
- [40] Surabhi Sachdev, Sarah Caudill, Heather Fong, Rico K. L. Lo, Cody Messick, Debnandini Mukherjee, Ryan Magee, Leo Tsukada, Kent Blackburn, Patrick Brady, Patrick Brockill, Kipp Cannon, Sydney J. Chamberlin, Deep Chatterjee, Jolien D. E. Creighton, Patrick Godwin, Anuradha Gupta, Chad Hanna, Shasvath Kapadia, Ryan N. Lang, Tjonnie G. F. Li, Duncan Meacher, Alexander Pace, Stephen Privitera, Laleh Sadeghian, Leslie Wade, Madeline Wade, Alan Weinstein, and Sophia Liting Xiao, “The GstLAL Search Analysis Methods for Compact Binary Mergers in Advanced LIGO’s Second and Advanced Virgo’s First Observing Runs,” *arXiv e-prints*, [arXiv:1901.08580 \(2019\)](#), [arXiv:1901.08580 \[gr-qc\]](#).
- [41] Gareth S. Davies, Thomas Dent, Márton Tápai, Ian Harry, Connor McIsaac, and Alexander H. Nitz, “Extending the PyCBC search for gravitational waves from compact binary mergers to a global network,” *Phys. Rev. D* **102**, 022004 (2020), [arXiv:2002.08291 \[astro-ph.HE\]](#).
- [42] F. Aubin, F. Brighenti, R. Chierici, D. Estevez, G. Greco, G. M. Guidi, V. Juste, F. Marion, B. Mours, E. Nitoglia, O. Sauter, and V. Sordini, “The MBTA pipeline for detecting compact binary coalescences in the third LIGO-Virgo observing run,” *Classical and Quantum Gravity* **38**, 095004 (2021), [arXiv:2012.11512 \[gr-qc\]](#).
- [43] B. P. Abbott, R. Abbott, T. D. Abbott, S. Abraham, F. Acernese, K. Ackley, A. Adams, C. Adams, R. X. Adhikari, V. B. Adya, and others, “Search for intermediate mass black hole binaries in the first and second observing runs of the Advanced LIGO and Virgo network,” *Phys. Rev. D* **100**, 064064 (2019), [arXiv:1907.09384 \[astro-ph.HE\]](#).
- [44] A. G. Abac, R. Abbott, H. Abe, F. Acernese, K. Ackley, C. Adamcewicz, S. Adhichary, *et al.*, “Search for Eccentric Black Hole Coalescences during the Third Observing Run of LIGO and Virgo,” *arXiv e-prints*, [arXiv:2308.03822 \(2023\)](#), [arXiv:2308.03822 \[astro-ph.HE\]](#).
- [45] Sashwat Tanay, Maria Haney, and Achamveedu Gopakumar, “Frequency and time-domain inspiral templates for comparable mass compact binaries in eccentric orbits,” *Phys. Rev. D* **93**, 064031 (2016), [arXiv:1602.03081 \[gr-qc\]](#).
- [46] E. A. Huerta, C. J. Moore, Prayush Kumar, Daniel George, Alvin J. K. Chua, Roland Haas, Erik Wessel, Daniel Johnson, Derek Glennon, Adam Rebei, A. Miguel Holgado, Jonathan R. Gair, and Harald P. Pfeiffer, “Eccentric, nonspinning, inspiral, Gaussian-process merger approximant for the detection and characterization of eccentric binary black hole mergers,” *Phys. Rev. D* **97**, 024031 (2018), [arXiv:1711.06276 \[gr-qc\]](#).
- [47] Alessandro Nagar, Alice Bonino, and Piero Retegno, “Effective one-body multipolar waveform model for spin-aligned, quasicircular, eccentric, hyperbolic black hole binaries,” *Phys. Rev. D* **103**, 104021 (2021), [arXiv:2101.08624 \[gr-qc\]](#).
- [48] Antoni Ramos-Buades, Alessandra Buonanno, Mohammed Khalil, and Serguei Ossokine, “Effective-one-body multipolar waveforms for eccentric binary black holes with nonprecessing spins,” *Phys. Rev. D* **105**, 044035 (2022), [arXiv:2112.06952 \[gr-qc\]](#).
- [49] Xiaolin Liu, Zhoujian Cao, and Zong-Hong Zhu, “A higher-multipole gravitational waveform model for an eccentric binary black holes based on the effective-one-body-numerical-relativity formalism,” *Classical and Quantum Gravity* **39**, 035009 (2022), [arXiv:2102.08614 \[gr-qc\]](#).
- [50] Xiaolin Liu, Zhoujian Cao, and Zong-Hong Zhu, “Effective-One-Body Numerical-Relativity waveform model for Eccentric spin-precessing binary black hole coalescence,” *arXiv e-prints*, [arXiv:2310.04552 \(2023\)](#), [arXiv:2310.04552 \[gr-qc\]](#).
- [51] Antoine Klein, “EFPE: Efficient fully precessing eccentric gravitational waveforms for binaries with long

- inspirals,” *arXiv e-prints*, [arXiv:2106.10291](#) (2021), [arXiv:2106.10291 \[gr-qc\]](#).
- [52] Isobel M. Romero-Shaw, Davide Gerosa, and Nicholas Loutrel, “Eccentricity or spin precession? Distinguishing subdominant effects in gravitational-wave data,” *MNRAS* **519**, 5352–5357 (2023), [arXiv:2211.07528 \[astro-ph.HE\]](#).
- [53] Yumeng Xu and Eleanor Hamilton, “Measurability of precession and eccentricity for heavy binary-black-hole mergers,” *Phys. Rev. D* **107**, 103049 (2023), [arXiv:2211.09561 \[gr-qc\]](#).
- [54] Isobel Romero-Shaw, Paul D. Lasky, Eric Thrane, and Juan Calderón Bustillo, “GW190521: Orbital Eccentricity and Signatures of Dynamical Formation in a Binary Black Hole Merger Signal,” *ApJ* **903**, L5 (2020), [arXiv:2009.04771 \[astro-ph.HE\]](#).
- [55] Alan M. Knee, Isobel M. Romero-Shaw, Paul D. Lasky, Jess McIver, and Eric Thrane, “A Rosetta Stone for Eccentric Gravitational Waveform Models,” *ApJ* **936**, 172 (2022), [arXiv:2207.14346 \[gr-qc\]](#).
- [56] Alice Bonino, Rossella Gamba, Patricia Schmidt, Alessandro Nagar, Geraint Pratten, Matteo Breschi, Piero Rettengo, and Sebastiano Bernuzzi, “Inferring eccentricity evolution from observations of coalescing binary black holes,” *Phys. Rev. D* **107**, 064024 (2023), [arXiv:2207.10474 \[gr-qc\]](#).
- [57] Md Arif Shaikh, Vijay Varma, Harald P. Pfeiffer, Antoni Ramos-Buades, and Maarten van de Meent, “Defining eccentricity for gravitational wave astronomy,” *Phys. Rev. D* **108**, 104007 (2023), [arXiv:2302.11257 \[gr-qc\]](#).
- [58] Aditya Vijaykumar, Alexandra G. Hanselman, and Michael Zevin, “Data release for “Consistent eccentricities for gravitational wave astronomy: Resolving discrepancies between astrophysical simulations and waveform models,” (2024).
- [59] Linqing Wen, “On the Eccentricity Distribution of Coalescing Black Hole Binaries Driven by the Kozai Mechanism in Globular Clusters,” *ApJ* **598**, 419–430 (2003), [arXiv:astro-ph/0211492 \[astro-ph\]](#).
- [60] Konstantinos Kritos, Vladimir Stokov, Vishal Baibhav, and Emanuele Berti, “Rapster: a fast code for dynamical formation of black-hole binaries in dense star clusters,” *arXiv e-prints*, [arXiv:2210.10055](#) (2022), [arXiv:2210.10055 \[astro-ph.HE\]](#).
- [61] Debatri Chattopadhyay, Jakob Stegmann, Fabio Antonini, Jordan Barber, and Isobel M. Romero-Shaw, “Double black hole mergers in nuclear star clusters: eccentricities, spins, masses, and the growth of massive seeds,” *MNRAS* **526**, 4908–4928 (2023), [arXiv:2308.10884 \[astro-ph.HE\]](#).
- [62] Antoine Klein, Yannick Boetzel, Achamvedu Gopakumar, Philippe Jetzer, and Lorenzo de Vittori, “Fourier domain gravitational waveforms for precessing eccentric binaries,” *Phys. Rev. D* **98**, 104043 (2018), [arXiv:1801.08542 \[gr-qc\]](#).
- [63] Adrian S. Hamers, “An Improved Numerical Fit to the Peak Harmonic Gravitational Wave Frequency Emitted by an Eccentric Binary,” *Research Notes of the American Astronomical Society* **5**, 275 (2021), [arXiv:2111.08033 \[gr-qc\]](#).
- [64] P. C. Peters and J. Mathews, “Gravitational Radiation from Point Masses in a Keplerian Orbit,” *Physical Review* **131**, 435–440 (1963).
- [65] Giulia Fumagalli and Davide Gerosa, “Spin-eccentricity interplay in merging binary black holes,” *Phys. Rev. D* **108**, 124055 (2023), [arXiv:2310.16893 \[gr-qc\]](#).
- [66] Wolfgang Junker and Gerhard Schaefer, “Binary systems - Higher order gravitational radiation damping and wave emission,” *MNRAS* **254**, 146–164 (1992).
- [67] Ronald Rieth and Gerhard Schäfer, “Spin and tail effects in the gravitational-wave emission of compact binaries,” *Classical and Quantum Gravity* **14**, 2357–2380 (1997).
- [68] A. Gopakumar and Bala R. Iyer, “Gravitational waves from inspiraling compact binaries: Angular momentum flux, evolution of the orbital elements, and the waveform to the second post-Newtonian order,” *Phys. Rev. D* **56**, 7708–7731 (1997), [arXiv:gr-qc/9710075 \[gr-qc\]](#).
- [69] K. G. Arun, Luc Blanchet, Bala R. Iyer, and Siddhartha Sinha, “Third post-Newtonian angular momentum flux and the secular evolution of orbital elements for inspiralling compact binaries in quasi-elliptical orbits,” *Phys. Rev. D* **80**, 124018 (2009), [arXiv:0908.3854 \[gr-qc\]](#).
- [70] Quentin Henry and Mohammed Khalil, “Spin effects in gravitational waveforms and fluxes for binaries on eccentric orbits to the third post-Newtonian order,” *Phys. Rev. D* **108**, 104016 (2023), [arXiv:2308.13606 \[gr-qc\]](#).
- [71] Carl L. Rodriguez, Newlin C. Weatherford, Scott C. Coughlin, Pau Amaro-Seoane, Katelyn Breivik, Sourav Chatterjee, Giacomo Fragione, Fulya Kiroğlu, Kyle Kremer, Nicholas Z. Rui, Claire S. Ye, Michael Zevin, and Frederic A. Rasio, “Modeling Dense Star Clusters in the Milky Way and beyond with the Cluster Monte Carlo Code,” *ApJS* **258**, 22 (2022), [arXiv:2106.02643 \[astro-ph.GA\]](#).
- [72] M. Hénon, “Monte Carlo Models of Star Clusters (Part of the Proceedings of the IAU Colloquium No. 10, held in Cambridge, England, August 12–15, 1970.),” *Ap&SS* **13**, 284–299 (1971).
- [73] M. H. Hénon, “The Monte Carlo Method (Papers appear in the Proceedings of IAU Colloquium No. 10 Gravitational N-Body Problem (ed. by Myron Lecar), R. Reidel Publ. Co., Dordrecht-Holland.),” (1971) pp. 151–167.
- [74] Kriten J. Joshi, Frederic A. Rasio, and Simon Portegies Zwart, “Monte Carlo Simulations of Globular Cluster Evolution. I. Method and Test Calculations,” *ApJ* **540**, 969–982 (2000), [arXiv:astro-ph/9909115 \[astro-ph\]](#).
- [75] Kriten J. Joshi, Cody P. Nave, and Frederic A. Rasio, “Monte Carlo Simulations of Globular Cluster Evolution. II. Mass Spectra, Stellar Evolution, and Lifetimes in the Galaxy,” *ApJ* **550**, 691–702 (2001), [arXiv:astro-ph/9912155 \[astro-ph\]](#).
- [76] J. M. Fregeau, M. A. Gürkan, K. J. Joshi, and F. A. Rasio, “Monte Carlo Simulations of Globular Cluster Evolution. III. Primordial Binary Interactions,” *ApJ* **593**, 772–787 (2003), [arXiv:astro-ph/0301521 \[astro-ph\]](#).
- [77] John M. Fregeau and Frederic A. Rasio, “Monte Carlo Simulations of Globular Cluster Evolution. IV. Direct Integration of Strong Interactions,” *ApJ* **658**, 1047–1061 (2007), [arXiv:astro-ph/0608261 \[astro-ph\]](#).
- [78] Sourav Chatterjee, John M. Fregeau, Stefan Umbreit, and Frederic A. Rasio, “Monte Carlo Simulations of Globular Cluster Evolution. V. Binary Stellar Evolution,” *ApJ* **719**, 915–930 (2010), [arXiv:0912.4682 \[astro-ph.GA\]](#).
- [79] Sourav Chatterjee, Stefan Umbreit, John M. Fregeau, and Frederic A. Rasio, “Understanding the dynamical state of globular clusters: core-collapsed versus non-core-collapsed,” *MNRAS* **429**, 2881–2893 (2013), [arXiv:1207.3063 \[astro-ph.GA\]](#).



- [80] Bharath Pattabiraman, Stefan Umbreit, Wei-keng Liao, Alok Choudhary, Vassiliki Kalogera, Gokhan Memik, and Frederic A. Rasio, “A Parallel Monte Carlo Code for Simulating Collisional N-body Systems,” *ApJS* **204**, 15 (2013), [arXiv:1206.5878 \[astro-ph.IM\]](#).
- [81] Carl L. Rodriguez, Meagan Morscher, Bharath Pattabiraman, Sourav Chatterjee, Carl-Johan Haster, and Frederic A. Rasio, “Binary Black Hole Mergers from Globular Clusters: Implications for Advanced LIGO,” *Phys. Rev. Lett.* **115**, 051101 (2015), [arXiv:1505.00792 \[astro-ph.HE\]](#).
- [82] Kyle Kremer, Claire S. Ye, Nicholas Z. Rui, Newlin C. Weatherford, Sourav Chatterjee, Giacomo Fragione, Carl L. Rodriguez, Mario Spera, and Frederic A. Rasio, “Modeling Dense Star Clusters in the Milky Way and Beyond with the CMC Cluster Catalog,” *ApJS* **247**, 48 (2020), [arXiv:1911.00018 \[astro-ph.HE\]](#).
- [83] Kyle Kremer, S Ye Claire, Nicholas Z Rui, Newlin C Weatherford, Sourav Chatterjee, Giacomo Fragione, Carl L Rodriguez, Mario Spera, and Frederic A Rasio, “Cluster monte carlo simulations,” (2020), accessed on 1-1-2023.
- [84] Carl L. Rodriguez, Pau Amaro-Seoane, Sourav Chatterjee, and Frederic A. Rasio, “Post-Newtonian Dynamics in Dense Star Clusters: Highly Eccentric, Highly Spinning, and Repeated Binary Black Hole Mergers,” *Phys. Rev. Lett.* **120**, 151101 (2018), [arXiv:1712.04937 \[astro-ph.HE\]](#).
- [85] Isobel Romero-Shaw, Paul D. Lasky, and Eric Thrane, “Four Eccentric Mergers Increase the Evidence that LIGO-Virgo-KAGRA’s Binary Black Holes Form Dynamically,” *ApJ* **940**, 171 (2022), [arXiv:2206.14695 \[astro-ph.HE\]](#).
- [86] Charles R. Harris, K. Jarrod Millman, Stéfan J. van der Walt, Ralf Gommers, Pauli Virtanen, David Cournapeau, Eric Wieser, Julian Taylor, Sebastian Berg, Nathaniel J. Smith, Robert Kern, Matti Picus, Stephan Hoyer, Marten H. van Kerkwijk, Matthew Brett, Allan Haldane, Jaime Fernández del Río, Mark Wiebe, Pearu Peterson, Pierre Gérard-Marchant, Kevin Shepard, Tyler Reddy, Warren Weckesser, Hameer Abbasi, Christoph Gohlke, and Travis E. Oliphant, “Array programming with NumPy,” *Nature* **585**, 357–362 (2020), [arXiv:2006.10256 \[cs.MS\]](#).
- [87] Pauli Virtanen, Ralf Gommers, Travis E. Oliphant, Matt Haberland, Tyler Reddy, David Cournapeau, Evgeni Burovski, Pearu Peterson, Warren Weckesser, Jonathan Bright, Stéfan J. van der Walt, Matthew Brett, Joshua Wilson, K. Jarrod Millman, Nikolay Mayorov, Andrew R. J. Nelson, Eric Jones, Robert Kern, Eric Larson, C. J. Carey, İlhan Polat, Yu Feng, Eric W. Moore, Jake VanderPlas, Denis Laxalde, Josef Perktold, Robert Cimrman, Ian Henriksen, E. A. Quintero, Charles R. Harris, Anne M. Archibald, Antônio H. Ribeiro, Fabian Pedregosa, Paul van Mulbregt, and SciPy 1.0 Contributors, “SciPy 1.0: fundamental algorithms for scientific computing in Python,” *Nature Methods* **17**, 261–272 (2020), [arXiv:1907.10121 \[cs.MS\]](#).
- [88] John D. Hunter, “Matplotlib: A 2D Graphics Environment,” *Computing in Science and Engineering* **9**, 90–95 (2007).
- [89] Astropy Collaboration, Thomas P. Robitaille, Erik J. Tollerud, Perry Greenfield, Michael Droettboom, Erik Bray, Tom Aldcroft, Matt Davis, Adam Ginsburg, Adrian M. Price-Whelan, Wolfgang E. Kerzendorf, Alexander Conley, Neil Crighton, Kyle Barbary, Demitri Muna, Henry Ferguson, Frédéric Grollier, Madhura M. Parikh, Prasanth H. Nair, Hans M. Unthert, Christoph Deil, Julien Woillez, Simon Conseil, Roban Kramer, James E. H. Turner, Leo Singer, Ryan Fox, Benjamin A. Weaver, Victor Zabalza, Zachary I. Edwards, K. Azalee Bostroem, D. J. Burke, Andrew R. Casey, Steven M. Crawford, Nadia Dencheva, Justin Ely, Tim Jenness, Kathleen Labrie, Pey Lian Lim, Francesco Pierfederici, Andrew Pontzen, Andy Ptak, Brian Refsdal, Mathieu Servillat, and Ole Streicher, “Astropy: A community Python package for astronomy,” *A&A* **558**, A33 (2013), [arXiv:1307.6212 \[astro-ph.IM\]](#).
- [90] Astropy Collaboration, A. M. Price-Whelan, B. M. Sipőcz, H. M. Günther, P. L. Lim, S. M. Crawford, S. Conseil, D. L. Shupe, M. W. Craig, N. Dencheva, A. Ginsburg, J. T. VanderPlas, L. D. Bradley, D. Pérez-Suárez, M. de Val-Borro, T. L. Aldcroft, K. L. Cruz, T. P. Robitaille, E. J. Tollerud, C. Ardelean, T. Babej, Y. P. Bach, M. Bachetti, A. V. Bakanov, S. P. Bamford, G. Barentsen, P. Barmby, A. Baumbach, K. L. Berry, F. Biscani, M. Bouchet, K. A. Bostroem, L. G. Bouma, G. B. Brammer, E. M. Bray, H. Breytenbach, H. Buddelmeijer, D. J. Burke, G. Calderone, J. L. Cano Rodríguez, M. Cara, J. V. M. Cardoso, S. Cheedella, Y. Copin, L. Corrales, D. Crichton, D. D’Avella, C. Deil, É. Depagne, J. P. Dietrich, A. Donath, M. Droettboom, N. Earl, T. Erben, S. Fabbro, L. A. Ferreira, T. Finethy, R. T. Fox, L. H. Garrison, S. L. J. Gibbons, D. A. Goldstein, R. Gommers, J. P. Greco, P. Greenfield, A. M. Groener, F. Grollier, A. Hagen, P. Hirst, D. Homeier, A. J. Horton, G. Hosseinzadeh, L. Hu, J. S. Hunkeler, Ž. Ivezić, A. Jain, T. Jenness, G. Kanarek, S. Kendrew, N. S. Kern, W. E. Kerzendorf, A. Khvalko, J. King, D. Kirkby, A. M. Kulkarni, A. Kumar, A. Lee, D. Lenz, S. P. Littlefair, Z. Ma, D. M. Macleod, M. Mastropietro, C. McCully, S. Montagnac, B. M. Morris, M. Mueller, S. J. Mumford, D. Muna, N. A. Murphy, S. Nelson, G. H. Nguyen, J. P. Ninan, M. Nöthe, S. Ogaz, S. Oh, J. K. Parejko, N. Parley, S. Pascual, R. Patil, A. A. Patil, A. L. Plunkett, J. X. Prochaska, T. Rastogi, V. Reddy Janga, J. Sabater, P. Sakurikar, M. Seifert, L. E. Sherbert, H. Sherwood-Taylor, A. Y. Shih, J. Sick, M. T. Silbiger, S. Singanamalla, L. P. Singer, P. H. Sladen, K. A. Sooley, S. Sornarajah, O. Streicher, P. Teuben, S. W. Thomas, G. R. Tremblay, J. E. H. Turner, V. Terrón, M. H. van Kerkwijk, A. de la Vega, L. L. Watkins, B. A. Weaver, J. B. Whitmore, J. Woillez, V. Zabalza, and Astropy Contributors, “The Astropy Project: Building an Open-science Project and Status of the v2.0 Core Package,” *AJ* **156**, 123 (2018), [arXiv:1801.02634 \[astro-ph.IM\]](#).
- [91] Thomas Kluyver, Benjain Ragan-Kelley, Fernando Pérez, Brian Granger, Matthias Bussonnier, Jonathan Frederic, Kyle Kelley, Jessica Hamrick, Jason Grout, Sylvain Corlay, Paul Ivanov, Damián Avila, Safia Abdalla, Carol Willing, and Jupyter Development Team, “Jupyter Notebooks—a publishing format for reproducible computational workflows,” in *IOS Press* (IOS Press, 2016) pp. 87–90.
- [92] Wes McKinney, “Data Structures for Statistical Computing in Python,” in *Proceedings of the 9th Python in Science Conference*, edited by Stéfan van der Walt and Jarrod Millman (2010) pp. 56 – 61.
- [93] Michael Waskom, “seaborn: statistical data visualization,” *The Journal of Open Source Software* **6**, 3021 (2021).



- [94] LIGO Scientific Collaboration, Virgo Collaboration, and KAGRA Collaboration, “**LVK Algorithm Library - LAL-Suite,**” Free software (GPL) (2018).